Mining of Mineral Deposits
Volume 17 (2023), Issue 4, 1-11

https://doi.org/10.33271/mining17.04.001

Deformation as a process to transform shape and volume of protective structures of the development mine workings during coal-rock mass off-loading

Daria Chepiga[1*], Iryna Bessarab[1], Vitalii Hnatiuk[2], Oleksandr Tkachuk[1], Oleksandr Kipko[1], Serhii Podkopaiev[1]

[1] *Donetsk National Technical University, Lutsk, Ukraine*
[2] *PJSC "Pokrovske Mine Management", Pokrovsk, Ukraine*

**Corresponding author: e-mail daria.chepiha@donntu.edu.ua*

Abstract

Purpose is to assess deformation characteristics of protective structures while coal-rock mass off-loading to ensure wall rock stability as well as operating conditions of the development mine workings in coal mines.

Methods. In a laboratory environment, uniaxial compression of protective structures has been applied on the models to identify the influence by deformation processes on the changes in their rigidness resulting from the shape and volume transformation.

Findings. Under the deformation of rigid structures in the context of a safe strain resource, potential energy of their changes in shape is 4.1-6.5 times higher than the one of changes in volume. Beyond the safe deformation resource when critical level of the specific potential strain energy has been exceeded, strength of protective structures is not sufficient to restrict wall rock movement limiting their use. If relative volume variation in the rigid protective structures is $\delta V > 0.06$-0.082 then they lose their stability. Under such conditions, structural rigidity decreases by 14-22%. If pliable wooden protective structures are used then relative $0.62 \le \delta V \le 0.72$ volume change doubles their rigidity. In the circumstances, the potential shape change energy is 2.1 times higher than the volume change energy; the abovementioned favours temporary compaction of wooden components of the compressive structure while improving its resistivity.

Originality. Regularities of changes in the specific potential deformation energy of protective structures depending upon their shape and volume variation in terms of uniaxial compression have been identified.

Practical implications. To ensure stability of wall rocks and maintain operating conditions of the development mine workings, it is reasonable to apply pliable wooden protective structures which will help restrict roof and floor movements after their compaction. Insufficient residual strength of rigid protective structures, resulting if they lose their stability, provokes rock failure within the working areas of coal mines.

Keywords: *deformation, rigidity, protective structures, development mine workings, uniaxial compression, bearing capacity, potential energy*

1. Introduction

Protection of the development mine workings is very important in the process of underground coal mining. Mine working stability supporting is among the key problems which solving influences heavily the technical and economic performance of mine activities as well as labour safety of personnel.

Mining deepening stipulated qualitative changes in geomechanical condition close to workings as well as intensification of rock pressure manifestations. Such a situation results in deformations of timbering of the development mine workings and significant increase in the expenditures connected with their maintenance during extraction operations. Average labour intensity of mine working support in Donbas mines is more than 82-85 man shifts per 1000 tons of coal output. Resupporting of mine workings is not a mechanized procedure; moreover, it decreases safety of the extraction activities.

The most complicated conditions are typical for the mine workings which, depending upon a mining procedure, are supported synchronously in the rock mass; in the zones of temporary bearing pressure and intensive rock displacement; in the zones of the stabilized rock pressure. State analysis of such mine workings shows that the arched support cannot compensate entirely the rock pressure impact. Maintenance of mine workings under such conditions is achieved through the efficiency of a protective procedure, which should provide continuity of wall rocks within the coal formation.

In many cases, stability of mine workings can be ensured at the expense of protective structures since they mitigate the impact by extraction operations as well as by negative manifestations of rock pressure relative to the peripheral rock mass. The abovementioned will make it possible to reduce deformation of the support. In this context, it is required to

Received: 20 June 2023. Accepted: 29 September 2023. Available online: 30 December 2023

Mining of Mineral Deposits. ISSN 2415-3443 (Online) | ISSN 2415-3435 (Print)

meet strength characteristics of wall rocks, and deformation characteristics of the protective structures. The problem solving needs assessment of deformation properties of the protective structures and their influence on the state of wall rocks upon which conditions of workings as well as personnel safety in a coal mine depend.

Coal mine deepening intensifies rock pressure manifestations within the workings. In the off-loading zones of coal-rock formation, clay rocks increase their volume and forms failure conditions; as a result, mine workings lose their stability [1]. Under such conditions, mine working protection by coal pillars, cast strip, and wood chocks cannot always ensure reliable defense of gate roads against negative manifestations of rock pressure.

It is known [2] that depending upon the rigidity characteristics, artificial safety devices are divided into stiff protective structures, i.e. coal pillars, cast strip, piers made of reinforced concrete blocks (BZBT), and their combinations. Pliable protective structures are rock packs, and wood chocks. As a rule, stiff protective structures and traditional objects of linear fracture mechanics considering brittle failure as a mechanism of accumulation of damages and fracture growth [3].

It is supposed [4] that in its stable state, no fracture growths if external load is constant while being less than some critical value. If the value increases, the deformed body initiates a process with generalization; according to the nonlinear dynamics terminology, the process provokes instability and failure [5]. It is obvious that internal potential energy of solid bodies under deformation has critical levels; during their transition, loose of stability takes place as well as behavioural changes.

Cast stripes can be considered as one of the efficient methods to protect workings if it is required to remain them in the mined-out area for the repeated use in the context of the combined and long-pillar extraction. Since the cast stripes together with BZBT piers belong to stiff protective structures, in general their application initiates increase in displacement value of foot rocks (so-called “stamp effect”; nevertheless, their stiffness provides roof rock “cutting”, and helps avoid formation of large consoles which pressure can worsen significantly the mine working state [6]. Among other activity reducing the effect [7], certain measures are applied intended to redistribute stresses within a mine working foot through the reshaping of protective structures. Namely, DonNTU experts have proposed to use the following: piers which form differs from rectangular [8]; a protective structure deepening into a mine working foot [9]; and arrangement schemes of protective structures with compensatory cavities [10]. It should be mentioned that in the real coal-rock formation, rigid protective structures are in the boundary stress-strain state. Their temporal potential decreases becoming insufficient to support the undermined rocks.

Analysis of the protective structures, used in coal mines, has shown that timber protection in the form of a wood chock is applied most of all [11], [12]. Imperfection of mechanical characteristics, slow resistance increase, and large value of the timbering pliability are significant disadvantages of such protective structures.

In the context of pliable protective structures, a deformation process in the material of a body being loaded is a complex procedure with the step-by-step development. First, mechanisms having low activating energy (i.e. elastic deformation) are implemented and then mechanisms having higher activating energy (i.e. plastic deformation) are used. For the purpose, stress-strain state of the body under deformation varies; the latter becomes the basis to assess its bearing capacity [13], [14].

It is worth mentioning that the assessment of bearing capacity of such pliable protective structure has to involve stress-strain modulus, which should not be equated with the elasticity modulus of the material. In the compression process, change in the stress-strain modulus will help assess both elastic and residual deformations of the body.

The experience, accumulated to analyze mechanical properties of samples under compression, shows that deformation characteristics are not sufficient to build a physical model of a solid body destruction; it especially concerns those ones experiencing even minor inelastic deformations. The process is followed by the external energy consumption or by its redistribution inside the body under deformation [15]. It is quite obvious that the destruction involves changes in the potential strain energy. At the same time, it should be taken into consideration what energy share is consumed to vary shape and volume of the deformed body to identify its temporal behaviour.

Relying upon the abovementioned, deformation should be considered as a process deforming both shape and volume of protective structures of development mine workings while coal-rock mass off-loading. Such an approach will make it possible to assess the impact of strain processes on the changes in the protective structure rigidness helping identify its bearing capacity in terms of a working area length. According to correspondence of strain characteristics of protective structures with strength properties of wall rocks in the coal-rock formation, facilities are provided to ensure operating conditions of development mine workings as well as labour safety of personnel.

The research purpose is to analyze deformation processes of the protective structures under uniaxial compression conditions taking into consideration their shape and volume transformation for the substantiated selection of a procedure protecting development workings in a coal mine.

To achieve the purpose, following tasks have been formulated:

– study strain processes of rigid protective structures (i.e. coal pillars, cast strip, piers made of reinforced concrete blocks (BZBT), and assess their bearing capacity;

– analyze strain processes of pliable wood protective structures (i.e. chocks, and sleeper chocks), and assess their bearing capacity;

– perform a comparative analysis of strain characteristics of the protective structures taking into consideration changes in their shape and volume under the conditions of uniaxial compression, and assess their impact on the wall rock stability in the coal-rock formation with the development mine workings.

2. Methods

The research object concerns deformation processes of the protective structures in the development mine workings in the process of coal-rock mass off-loading.

Analysis of strain processes as well as changes in rigidness of the protective structures in the development mine workings under the conditions of uniaxial compression involved studies with the use of experimental samples represented in the form of coal pillars, cement blocks, cast strip, and BZBT piers.

Pliable wood protective structures were represented in the form of chocks, and sleeper chocks. Dimensions of the experimental samples are as follows: h_0 = 0.04 m being the initial height; and $S = a \cdot b$ = 0.04·0.04 = 0.0016 square meters being a cross-sectional area. Simulation scale is M 1:25.

Experimental samples were mounted between the roof and floor represented as a beam with h_b = 0.02 m thickness, l_b = 0.08 m length, and b_b = 0.04 m width.

Figure 1 demonstrates general view of the experimental samples.

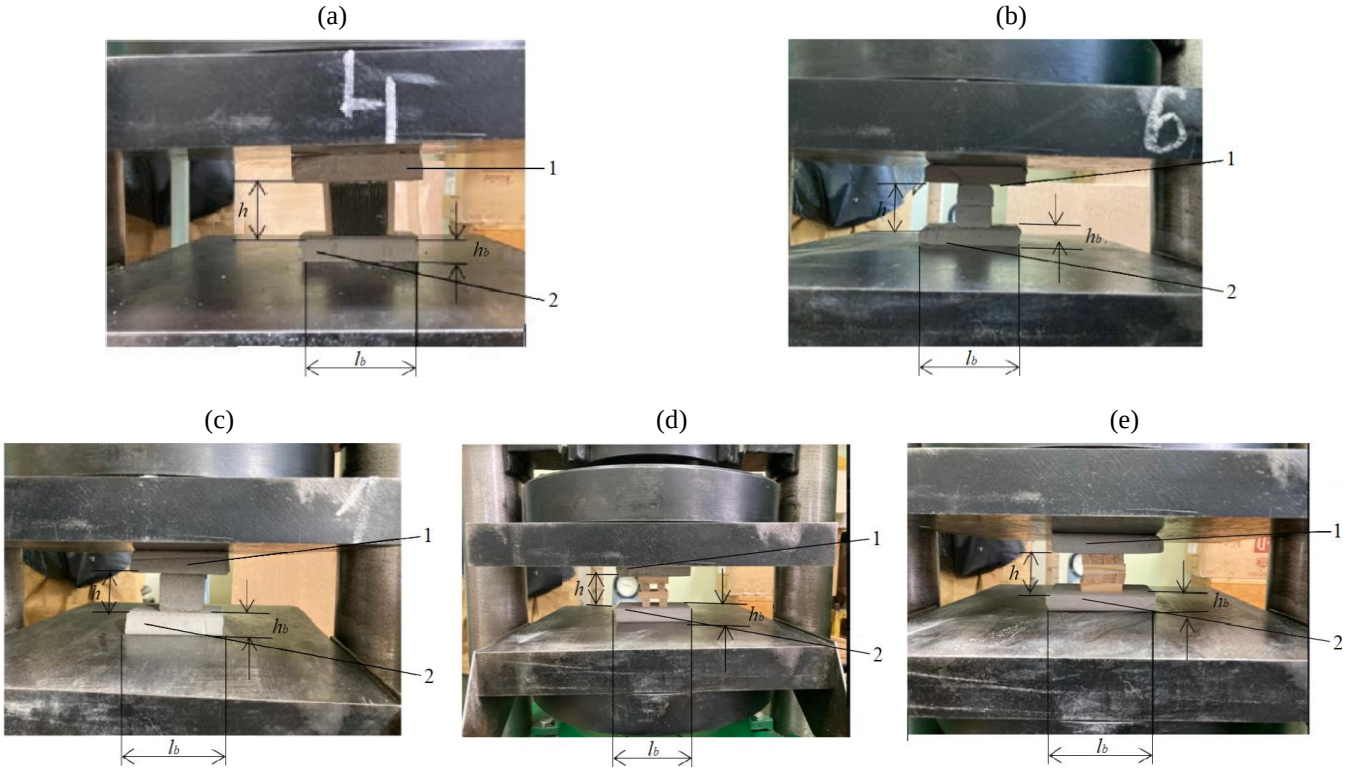

Figure 1. General view of the experimental samples in the form of: (a) coal pillars; (b) cement blocks; (c) BZBT piers; (d) wood chocks; (e) wood sleeper chocks; 1 and 2 – beam as a roof and floor model; h – sample height, m; h_b – beam width, m; l_b – beam length, m

The research provided equity of balance nature and model equations [16]-[19]. Compression strength of the models was defined with the help of the Expression [13], [14], [20], [21]:

$$\sigma_{com}^{m} = \frac{l_m}{l_n} \cdot \frac{\gamma_m}{\gamma_n} \cdot \sigma_{com}^{n}, \quad (1)$$

where:

σ_{com}^{m} and σ_{com}^{n} – are compression strength of model and nature respectively, N/m^2;

l_m and l_n – linear dimensions of model and mature, m;

γ_m and γ_n – density of a model and nature materials, kg/m^3.

Table 1 explains characteristics of the materials for the experimental samples. Table 2 lists characteristics of wood applied for the protective structures.

To ensure the mechanical model-nature identity, balance of weight parameters was ignored; it is quite permissible [22].

The experimental samples in the form of models of protective structures experienced uniaxial compression with the help of П-50 press. During the experiments, strain of Δh, m samples was registered from a compressive force value F (kN). A moment of rigidity reduction c (N/m) was recorded for experimental samples in the form of coal pillars, cast strip, cement blocks, and BZBT piers. As for wood chocks, and sleeper chocks, external load was applied against the grain.

Under uniaxial compression, relative strain of experimental samples was defined through the Expression [23]:

$$\lambda = \frac{\Delta h}{h_0}. \quad (2)$$

Table 1. Characteristics of the materials

Object	Material	γ, kg/m^3	σ_c, MPa
	Coal pillar		
Model	Sand-cement mixture added by resina	1100	0.4
Nature	Coal	1300	1.2
	Cement blocks		
Model	Sand-cement mixture	1700	1.06
Nature	Concrete	2300	36.0
	Cast strip		
Model	Sand-cement mixture	1780	1.39
Nature	Cement with hardener	2560	50.0
	BZBT piers		
Model	Sand-cement mixture with hardener	1800	1.43
Nature	Cement with hardeners for reinforcement	2610	52.0
	Wall rocks		
Model	Sand-cement mixture	1600	1.33
Nature	Aleurite	2300	48.0

Table 2. Physicomechanical characteristics of wood

Type	Compressive strength σ_c, MPa		Poisson ratio	
	Along the grain	Against the grain	Along the grain	Against the grain
Pine	85	86	0.50	0.02

Rigidity of the experimental samples was identified like in [24]:

$$c = \frac{F}{\Delta h}. \quad (3)$$

Relative changes in δV value of the experimental samples under the conditions of uniaxial compression were determined using the Expression [25]:

$$\delta V = (1-2\nu)\cdot\lambda, \quad (4)$$

where:

ν – the Poisson ratio.

Strain modulus E_d of protective structures was identified relying upon Hooke's law, and applying the Formula [25]:

$$E_d = \sigma\cdot\frac{h_0}{\Delta h}, \quad (5)$$

where:

$\sigma = F / S$ – mechanical stress considered as pressure under uniaxial compression, N/m^2.

External force, consumed to deform samples, can be determined through [25] Formula:

$$A = \frac{E_d\cdot V}{2}\cdot\lambda^2, \quad (6)$$

where:

V – the sample volume, m^3.

Strain of experimental samples consumes external forces to change their shape and volume. It is known [25], [26] that potential energy of protective structures can be divided into the energy varying a shape:

$$U_f = \frac{(1+\nu)}{3E_d}\cdot\sigma^2, \quad (7)$$

and the energy varying volume [21], [27]:

$$U_v = \frac{(1-2\nu)}{6E_d}\cdot\sigma^2. \quad (8)$$

Quantity of energy U (J), accumulated by the sample, may be defined through the Expression [25], [28]:

$$U = \frac{\sigma^2}{2E_d}\cdot V, \quad (9)$$

where:

$\sigma^2 / 2E_d$ – the specific potential energy deforming experimental samples, J/m^3.

It is supposed [25], [26] that internal potential energy of the objects of mechanics of a solid deformed body has several critical levels of potential strain energy.

Experimental samples vary their behaviour during transition of the critical level of the specific potential deformation energy [25]. It is obvious that their stress-strain state also experiences certain changes.

3. Results and discussion

3.1. Research results concerning deformation processes of brittle protective structures

Experimental samples in the form of coal pillars, cast strip, cement blocks, and BZBT piers were considered; they experienced uniaxial compression. Table 3 shows the research results concerning analysis of deformation processes under static loading of the models and boundary value of external loading F (kN) which provides the model stability. The value matches the specific potential strain energy $\sigma^2 / 2E_d$ (MJ/m^3); relative change in δV volume; and performance of A compression (J).

Figure 2 shows a graph of changes in relative strain λ and rigidity c (N/m) of the experimental samples in the form of coal pillars depending upon the external loading value F (kN) under the conditions of uniaxial compression.

Table 3. Research results concerning deformation processes under static loading of the rigid protective structures

Protective structure type	ν	F, kN	λ	σ, MPa	$\sigma^2 / 2E_d$, MJ/m^3	δV	A, J	U_f / U_v	U_f	U_v
Coal pillars	0.30	15	0.15	9.3	0.70	0.06	45	6.5	0.609	0.099
Cast strip	0.20	44	0.13	27.5	1.78	0.078	114	4.1	1.43	0.35
Cement blocks	0.22	42	0.12	26.2	1.96	0.082	126	4.3	1.60	0.36
BZBT piers	0.26	49	0.12	30.6	1.91	0.06	122	5.2	1.60	0.30

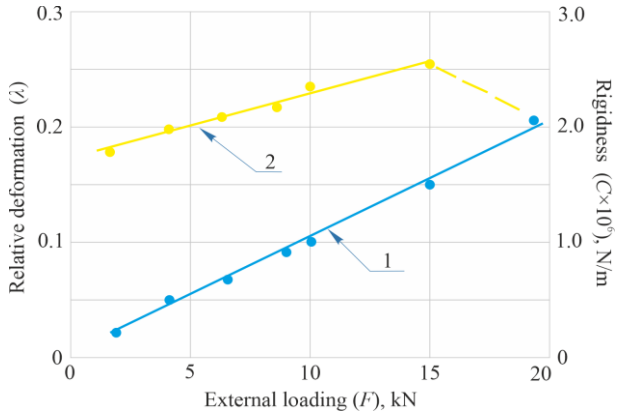

Figure 2. Graphs of relative deformation λ and rigidity c (N/m) of the experimental samples in the form of coal pillars depending upon the external force value F (kN) under the conditions of uniaxial compression: 1 – λ; 2 – c

It has been recorded that F = 2 kN up to F = 19 kN increase in external loading factors into λ = 0.027 to λ = 0.2 change in relative deformation (Fig. 2, curve *1*). Within F = 2 kN up to F = 15 kN interval of change in loading value, rigidity of experimental samples was increasing from $c = 1.81\cdot10^6$ N/m to $c = 2.5\cdot10^6$ N/m; then it was decreasing down to $c = 2.1\cdot10^6$ N/m under F = 19 kN (Fig. 2, curve *2*).

Figure 3 demonstrates graphs of changes in relative deformation λ and rigidity c (N/m) of the experimental samples in the form of BZBT piers, cast strip, and cement blocks depending upon the external loading value F (kN) under the conditions of uniaxial compression.

It has been recorded that in the context of the applied protective structures, increase of the external loading F (kN) results in relative deformation λ growth (Fig. 3). As for experimental samples in the form of BZBT piers, F = 10 kN up to F = 56 kN changes in external loading factors into λ = 0.03 to λ = 0.17 relative deformation growth (Fig. 3, curve *1*). In this vein, an increse in the sample rigidity is recorded in a 10 kN $\le F \le$ 49 kN range of loading values from $c = 8.3\cdot10^6$ N/m up to $c = 9.8\cdot10^6$ N/m; its drop down $c = 8.0\cdot10^6$ N/m is recorded if F = 56 kN (Fig. 3, curve *4*). In terms of the experimental samples in the form of a cast strip, F = 10 kN to F = 50 kN changes in the external loading increase relative deformation from λ = 0.0 up to λ = 0.17 (Fig. 3, curve *2*).

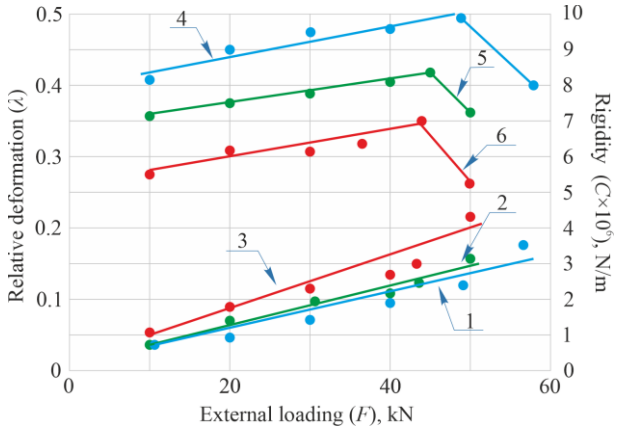

Figure 3. Graphs of changes in relative deformation λ and rigidity c (N/m) of the experimental samples depending upon the external loading value F (kN) under the conditions of uniaxial compression: 1, 4 – BZBT piers; 2, 5 – cast strips; 3 and 6 – cement blocks; 1, 2, 3 – λ; 4, 5, 6 – c (N/m)

Moreover, rigidity of the samples, growing from $c = 7.1 \cdot 10^6$ N/m to $c = 8.4 \cdot 10^6$ N/m, is recorded in the $0.03 \le \lambda \le 0.13$ range of relative deformation when the external loading is $F \le 44$ kN. If $F = 50$ kN then rigidity of the samples decreases down to $c = 7.03 \cdot 10^6$ N/m (Fig. 3, curve *5*).

If uniaxial compression of the experimental samples in the form of cement blocks takes place then $F = 10$ kN to $F = 50$ kN change in external loading factors into $\lambda = 0.04$ up to $\lambda = 0.22$ increase of relative deformation (Fig. 3, curve *3*). Growth of the sample rigidity from $c = 5.5 \cdot 10^6$ N/m to $c = 7.0 \cdot 10^6$ N/m has been recorded within 10 kN $\le F \le$42 kN range of external loading action; its decrease down to $c = 5.5 \cdot 10^6$ N/m value has been recorded under $F = 50$ kN (Fig. 3, curve *6*).

Figure 4 shows dependencies of changes in height Δh (m) of the experimental samples depending upon mechanical stress σ (MPa) under the conditions of uniaxial compression.

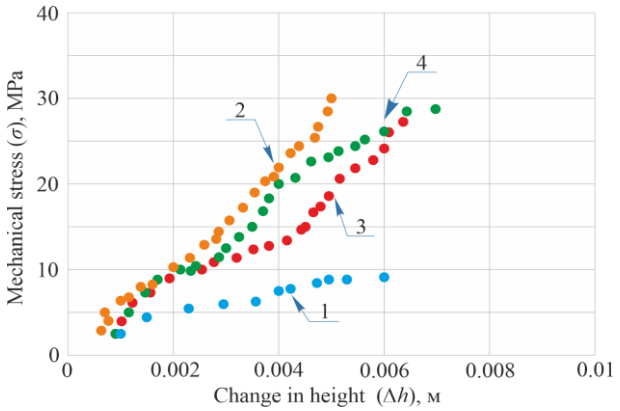

Figure 4. Graphs of change in Δh (m) height of the experimental samples in the form of coal pillars (1); BZBT piers (2); cement blocks (3); and cast strip (4) mechanical stress value σ (MPa) under the conditions of uniaxial compression

Compression diagram of the experimental samples is represented by a dependence between mechanical stress σ (MPa) growth and Δh (m) deformations (Fig. 4). All the tests ended in the destruction of the samples: $\sigma = 11.8$ MPa for coal pillars (Fig. 4, curve *1*); $\sigma = 30.6$ MPa for BZBT piers (Fig. 4, curve *2*); $\sigma = 26.2$ MPa for cement blocks (Fig. 4, curve *3*); and $\sigma = 27.5$ MPa for a cast strip (Fig. 4, curve *4*).

Figure 5 is general view of the samples after they lost their stability. Figure 6 demonstrates graphs of relative changes in δV volume of the experimental samples depending upon mechanical stress value σ (MPa) under the conditions of uniaxial compression.

Relying upon the tests, following linear dependence has been established between relative changes in volume δV of the experimental samples and mechanical stress σ (MPa) under the conditions of uniaxial compression:

$$\sigma = a \cdot \delta V + b\,, \qquad (10)$$

where correlation coefficient is $R^2 = 0.98$-0.99.

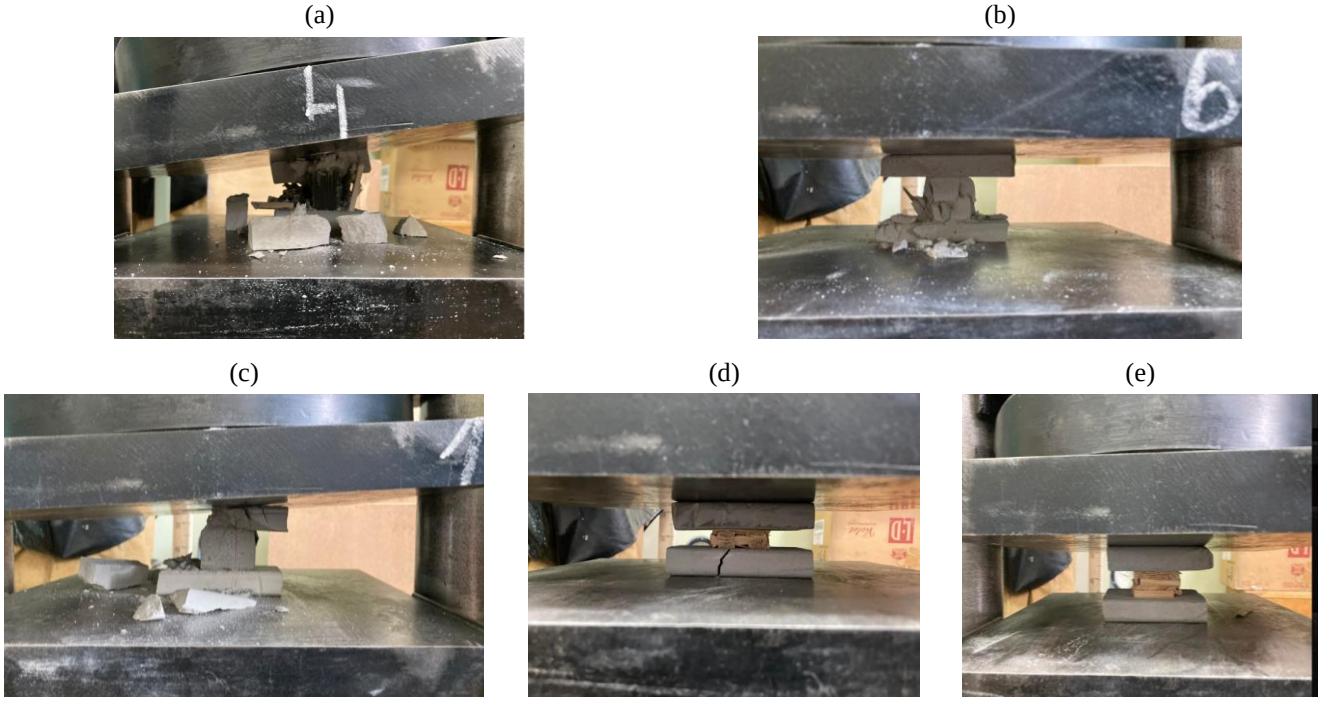

Figure 5. General view of the experimental samples in the form of: (a) coal pillars; (b) cement blocks; (c) BZBT piers; (d) wood chocks; (e) sleeper chocks: (a)-(c) – stability loss moment; (d) and (e) – a moment of compression initiation

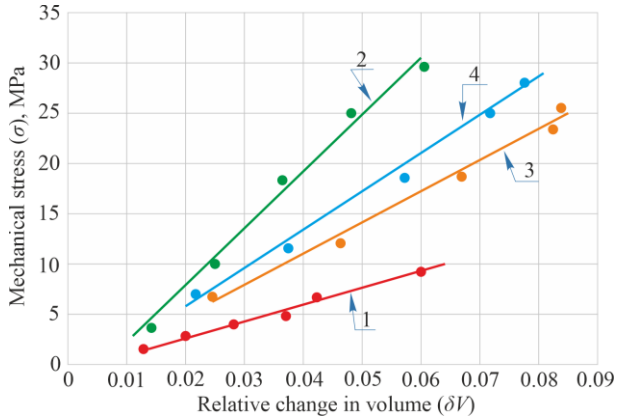

Figure 6. Graphs of relative changes in δV volume of the experimental samples in the form of coal pillars (1); BZBT piers (2); cement blocks (3); and a cast stripe (4) depending upon mechanical stress value σ (MPa) under the conditions of uniaxial compression

To identify the dependence type, the known techniques for experimental data processing were applied [29], [30].

Table 4 shows values of *a* and *b* coefficients for the experimental samples.

Table 4. Values of a and b coefficients in terms of a linear dependence between mechanical stress σ and relative change in volume δV

Experimental sample	σ, MPa	δV	Coefficient values	
			a	*b*
Coal pillars	9.37	0.06	165.516	-0.802
BZBT piers	30.6	0.06	532.159	-1.186
Rock blocks	26.5	0.082	330.437	-2.478
Cast strip	27.5	0.078	372.015	-1.875

Table 4 explains that growth in mechanical stress σ (MPa) factors into increase of a and b coefficients. In this context, relative $\delta V = 0.06$ up to $\delta V = 0.082$ increase in volume of the experimental samples takes place.

3.2. Findings of strain processes of wood pliable protective structures

Experimental wood samples in the form of chocks and sleeper chocks were considered. Table 5 demonstrates findings of strain processes under static loading of the samples, and boundary values of external loading (kN) under which action the models experienced compaction. The specific potential deformation energy value $\sigma^2 / 2\,E_d$ (MJ/m^3), relative change in volume δV, and compression A (J) correspond to the value.

Figure 7 shows graphs in changes of relative deformation λ and c rigidness (N/m) of wood experimental samples depending upon the external loading F (kN) value under the conditions of uniaxial compression.

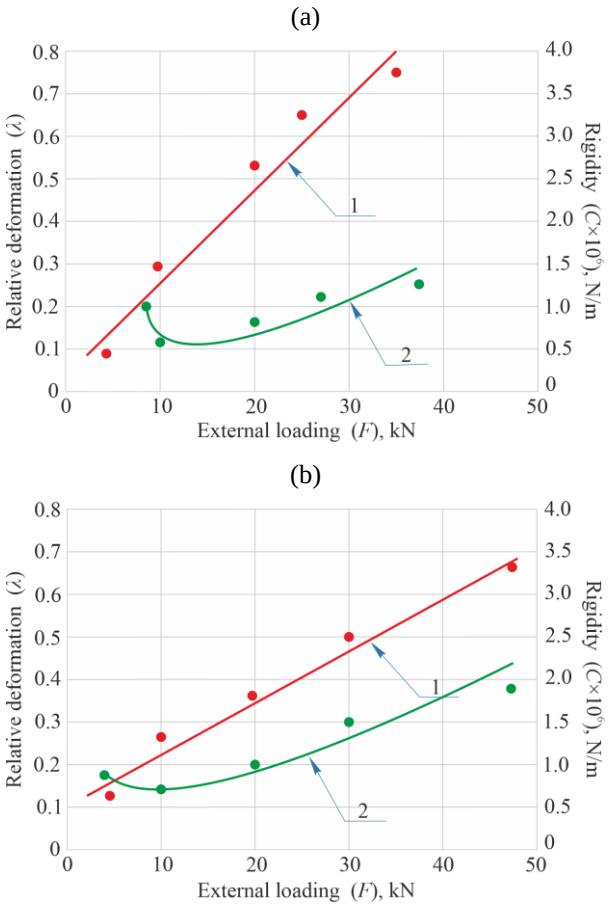

Figure 7. Graphs of changes in relative deformation λ and c rigidity (N/m) of wood experimental samples depending upon external loading F (kN) value under the conditions of uniaxial compression: (a) wood chocks; (b) sleeper chock; 1 – λ; and 2 – c

$\lambda = 0.2$ up to $\lambda = 0.75$ increase in relative deformation of the experimental samples in the form of wood chocks has been recorded if the external loading growth is $F = 8$ kN to $F = 35$ kN (Fig. 7, curve *1*). In this context, rigidity of the external samples, experiencing $F = 8$ kN external loading, is $c = 1.0 \cdot 10^6$ N/m; its growth up to $F = 35$ kN results in the rigidity increase up to $c = 1.16 \cdot 10^6$ N/m (Fig. 7a, curve *2*).

As for the experimental samples in the form of sleeper chocks, $F = 8$ kN up to $F = 49$ kN increase in the external loading factors into $\lambda = 0.12$ to $\lambda = 0.65$ relative strain variation (Fig. 7b, curve *1*).

In this case, rigidity of the experimental samples at an initial stage of compressive loading drops from $c = 1.0 \cdot 10^9$ N/m down to $c = 0.9 \cdot 10^6$ N/m with following increase up to $c = 1.88 \cdot 10^6$ N/m (Fig. 7b, curve *2*).

Table 5. The research results concerning strain processes under static loading of wood protective structures

Protective structures type	ν	F, kN	λ	σ, MPa	$\sigma^2 / 2\,E_d$, MJ/m^3	δV	A, J	U_f / U_v	U_f, MJ/m^3	U_v, MJ/m^3
Wood chock	0.02	35	0.75	21.8	8.2	0.72	525	2.12	5.57	2.62
Sleeper chock	0.02	49	0.65	30.6	9.95	0.62	637	2.12	6.76	3.18

Figure 8 shows graphs of changes in deformation value Δh (m) of experimental wood samples depending upon mechanical stress σ (MPa) under the conditions of uniaxial compression.

Increasing deformation value Δh (m), depending upon mechanical stress value σ (MPa), has been recorded. A deformation value grows from $\Delta h = 0.008$ m to $\Delta h = 0.003$ m for wood chocks if mechanical strain experiences $\sigma = 3.0$ MPa – $\sigma = 21.8$ MPa increase (Fig. 8, curve *1*). As for sleeper chocks, $\sigma = 3.12$ MPa up to $\sigma = 30.6$ MPa mechanical stress growing results in Δh=0.005 m-Δh=0.026 m increase in deformation value (Fig. 8, curve *2*).

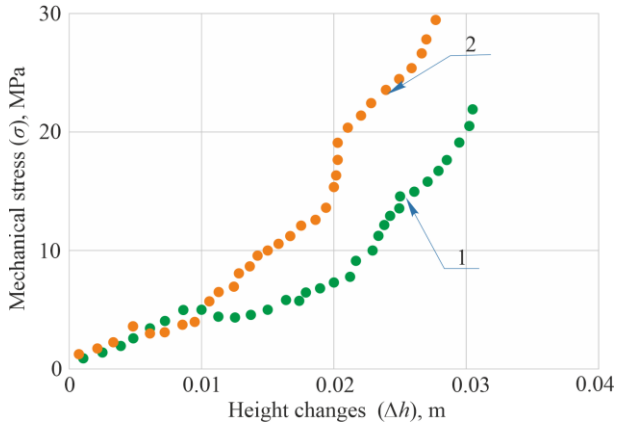

Figure 8. Graphs of changes in relative deformation Δh (m) of the experimental wood samples depending upon mechanical stress σ (MPa) under the conditions of uniaxial compression: 1 – chocks; 2 – sleeper chocks

Increasing deformation value Δh (m), depending upon mechanical stress value σ (MPa), has been recorded. A deformation value grows from $\Delta h = 0.008$ m to $\Delta h = 0.003$ m for wood chocks if mechanical strain experiences $\sigma = 3.0$ MPa – $\sigma = 21.8$ MPa increase (Fig. 8, curve *1*). As for sleeper chocks, $\sigma = 3.12$ MPa up to $\sigma = 30.6$ MPa mechanical stress growing results in $\Delta h = 0.005$ m – $\Delta h = 0.026$ m increase in deformation value (Fig. 8, curve *2*).

Figure 9 demonstrates graphs of relative changes in volume δV of the experimental wood samples depending upon mechanical stress value σ (MPa) under the conditions of uniaxial compression.

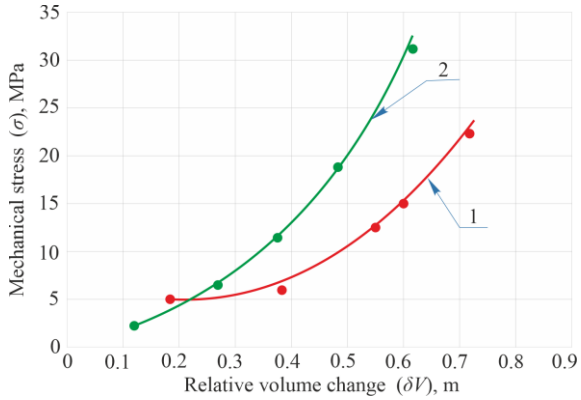

Figure 9. Graphs of relative changes in δV volume of the experimental wood samples depending upon mechanical stress value σ (MPa) under the conditions of uniaxial compression: 1 – chock; 2 – sleeper chock

If mechanical stress σ (MPa) increases then relative δV volume value grows as well. As for wood chocks, $\sigma = 5.0$ MPa – $\sigma = 21.8$ MPa mechanical stress increase factors into relative $\delta V = 0.19$ – $\delta V = 0.72$ volume change (Fig. 9, curve *1*). In the context of sleeper chocks, $\sigma = 3.12$ MPa – $\sigma = 30.6$ MPa increase of mechanical stress results in $\delta V = 0.12$ – $\delta V = 0.62$ growth of relative volume change (Fig. 9, curve *2*).

After the experimental data have been processed [29], [30], following exponential dependence was identified between the determined values:

$\sigma = e^{0.9248 + 2.9398\ \delta V}$ for wood chocks;

$\sigma = e^{0.6224 + 4.6417\ \delta V}$ for sleeper chocks;

$R^2 = 0.98$ correlation coefficient.

3.3. Assessment of deformation characteristics of the protective structures taking into consideration changes in shape, volume, and rigidity to substantiate safety procedure for mine workings

Figure 10 demonstrates graph of relative volume δV change depending upon longitudinal strain λ under the conditions of uniaxial compression.

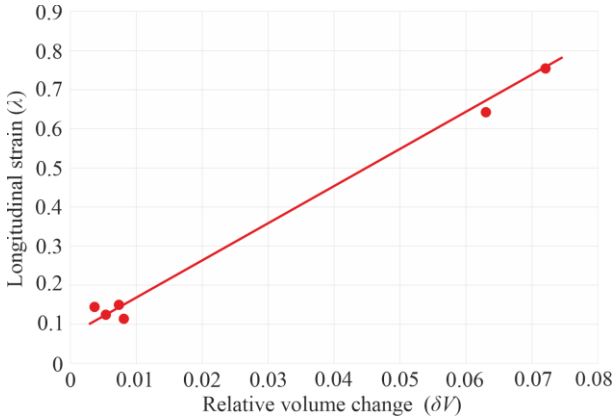

Figure 10. Graph of relative volume δV change depending upon longitudinal strain λ under the conditions of uniaxial compression

The graph helps understand that $\lambda = 0.12$ up to $\lambda = 0.75$ increase in longitudinal strain, recorded under static loading of experimental samples, results in the relative $\delta V = 0.06$ – $\delta V = 0.72$ volume growth (Fig. 10).

Figure 11 represents graph of the specific potential $\sigma^2 / 2\ E_d$ strain energy change of the experimental samples depending upon lateral deformation coefficient *v*.

It has been recorded that $v = 0.3$ – $v = 0.02$ decrease in the lateral deformation coefficient results in $\sigma^2 / 2\ E_d = 0.7$ MJ/m^3 – $\sigma^2 / 2\ E_d = 9.95$ MJ/m^3 increase of the specific potential strain (Fig. 11).

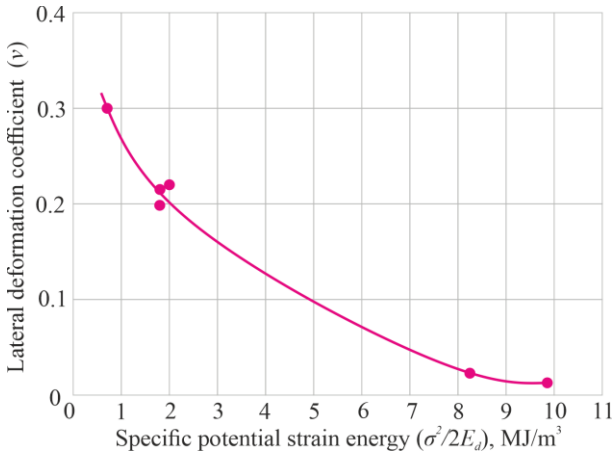

Figure 11. Graph of the specific potential σ² / 2 E_d strain energy change of the experimental samples depending upon lateral deformation coefficient v

Figure 12 shows graph of changes in *A* compression of the experimental samples depending upon the specific potential deformation energy $\sigma^2 / 2\ E_d$.

The graph explains that $A = 45$ J – $A = 637$ J compression intensification initiates increase in the specific potential deformation energy of the experimental samples from $\sigma^2 / 2\ E_d = 0.7$ MJ/m^3 up to $\sigma^2 / 2\ E_d = 9.95$ MJ/m^3 (Fig. 12).

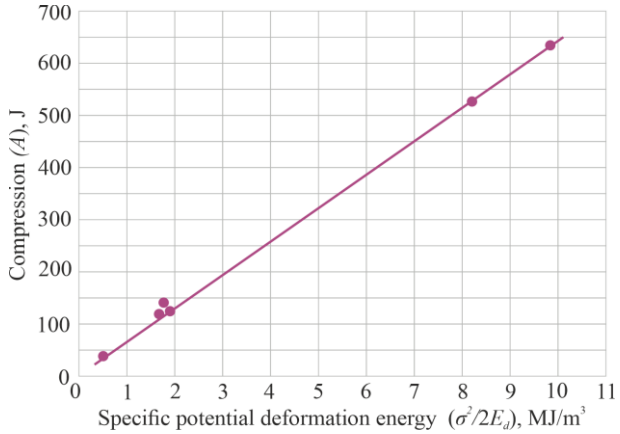

Figure 12. Graph of changes in A compression of experimental samples depending upon the specific potential deformation energy $\sigma^2 / 2\ E_d$ under the conditions of uniaxial compression: 1 – U_f; 2 – U_v

Figure 13 represents summary graphs of changes in the specific potential deformation energy $\sigma^2 / 2\ E_d$ of the experimental graphs depending upon the potential energy of shape variation U_f and potential energy of volume variation U_v under the conditions of uniaxial compression.

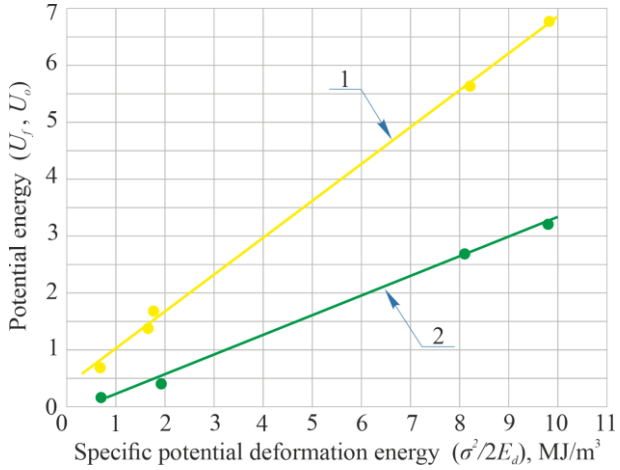

Figure 13. Graph of change in the specific potential deformation energy $\sigma^2 / 2\ E_d$ of the experimental samples depending: 1 – upon potential energy of change in shape U_f; 2 – under potential energy of change in volume U_v

It is seen from the graphs that owing to intensification of the potential energy of shape change of the experimental samples from $U_f = 0.609$ to $U_f = 6.76$ MJ/m^3 results in the increased potential deformation energy, i.e. from $\sigma^2 / 2\ E_d = 0.7$ MJ/m^3 up to $\sigma^2 / 2\ E_d = 9.95$ MJ/m^3. Within the interval of changes in $\sigma^2 / 2\ E_d$ parameter, $U_v = 0.093$ to $U_v = 3.18$ MJ/m^3 increase in the potential energy of change in volume is also recorded (Fig. 13).

Figure 14 demonstrates a graph of changes in the specific potential strain energy of the experimental samples $\sigma^2 / 2\ E_d$ depending upon U_f / U_v ratio taking into consideration potential energy of change in shape U_f as well as potential energy of change in volume U_v under the conditions of uniaxial compression.

It becomes clear from the graph that the decreased potential energy of changes in shape-potential energy of changes in volume ratio (i.e. $U_f / U_v = 6.5$ down to $U_f / U_v = 2.12$) factors into the increased specific potential strain energy (i.e. $\sigma^2 / 2\ E_d = 0.7$ MJ/m^3 up to $\sigma^2 / 2\ E_d = 9.95$ MJ/m^3) (Fig. 14).

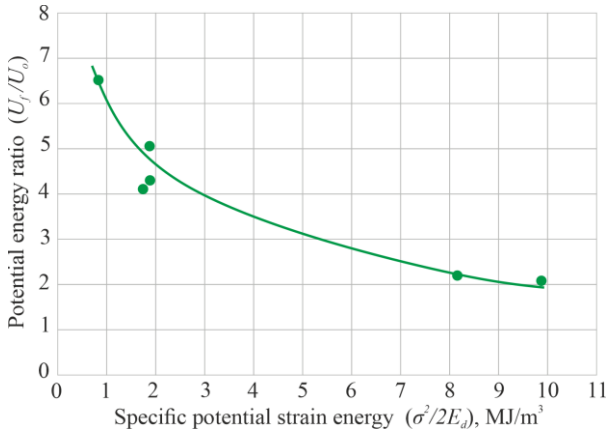

Figure 14. Graph of changes in the specific potential strain energy $\sigma^2 / 2\ E_d$ of the experimental samples depending upon U_f / U_v ratio taking into consideration potential energy of change in shape U_f as well as potential energy of change in volume U_v under the conditions of uniaxial compression

It has been turned out after the experimental data processing [23], [24] that there is an exponential dependence of the type:

$$\frac{U_f}{U_v} = e^{1.7767 - 0.1209 \frac{\sigma^2}{2E_d}}, \quad (11)$$

with 0.95 correlation coefficient.

Figure 15 shows graph of changes in U_f / U_v ratio (i.e. between potential energy of changes in shape U_f and potential energy of changes in volume U_v) of the experimental samples depending upon their longitudinal strain Δh (m) under the conditions of relative compression.

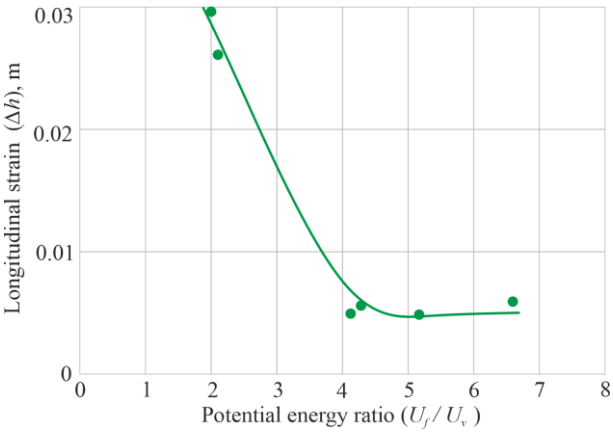

Figure 15. Graph of changes in U_f / U_v ratio (i.e. between potential energy of changes in shape U_f, and potential energy of changes in volume Uv) of the experimental samples depending upon their longitudinal strain Δh (m) under the conditions of relative compression

The graph explains that longitudinal strain intensification Δh (m) decreases U_f / U_v ratio; under maximum $\Delta h = 0.03$ values it corresponds to $U_f / U_v = 2.1$. Consequently, the potential energy of changes in shape is 2.1 times higher than the one in volume which is typical for the pliable protective structures. If longitudinal strain is of minimum value (i.e. $\Delta h = 0.005$ m) then the ratio demonstrates its peak value being $U_f / U_v = 9.95\ U_v$ which is typical for the rigid protective structures (Fig. 15).

It should be mentioned that under the conditions of uniaxial compression Δh (m) strain was studied in terms of which external forces F (kN) performed A operation (J). Relying upon the energy conservation law, the operation transformed into potential energy consumed to vary both shape and volume of the experimental samples. The deformed body behaviour was studied while recording relative changes in δV volume. Rigidity degree depended upon strain value Δh (m) resulting from compression.

The findings have helped identify impact of deformation processes on the changes in shape, volume, and rigidity of protective structures; the abovementioned helps assess their bearing capacity. Safe deformation resource has been determined for rigid protective structures under changes in relative strain; the resource is $0.12 \le \lambda \le 0.15$. In the range of the safe deformation resource, 6.0-8.2% volume increase of experimental samples as well as their rigidity is observed. Potential energy of shape variation U_f is 4.1-6.5 times higher than potential energy of volume variation U_v. In this context, mechanical stress intensification makes longitudinal strain Δh achieve its maximum values (Fig. 4) which helped provide stability of compressive structures.

It has been recorded that if relative volume change is $\delta V >$ 0.006-0.082 then relative deformation λ of the experimental samples increases (Fig. 3, dependencies 1, 2, and 3), and rigidity experiences its 14-22% decrease (Fig. 3, dependencies 4, 5, and 6). Consequently, protective structures lose their stability, and their bearing capacity reduces. Under the conditions when protective structures are beyond their safe deformation resource, and critical level of the specific potential strain energy is exceeded, strength of the protective structures is not sufficient to restrict displacement of the simulated wall rocks.

As for pliable wood protective structures, $0.65 \le \lambda \le 0.75$ changes in relative deformation as well as $0.62 \le \lambda \le 0.72$ in relative changes in volume, double rigidity increase has been recorded. Under such conditions, potential energy of shape change U_f is 2.1 higher than potential energy of volume change U_v; moreover, the specific potential strain energy $\sigma^2 / 2 E_d$ achieves its maximum values. The process is followed by compaction of structural wood components and their bearing capacity improvement. Compaction of wood chocks is followed by their increased rigidity as well as resistivity (Fig. 7a, b).

Potential energy of shape change U_f – potential energy of volume change U_v ratio of the experimental samples under the conditions of uniaxial compression depends upon lateral strain coefficient υ. It follows from Expressions (7), (8). It has been defined that in the context of rigid protective structures, the potential energy of shape change exceeds the potential energy of volume change. As for such constructions, safety limit of deformation resource of protective structures is the critical level of the specific potential strain energy.

During deformation of wood pliable protective structures, the potential energy of shape change U_f slightly exceeds the potential energy of volume change U_v. Meanwhile, external loading should be applied across grain of the structure components. In terms of the safe resource deformation, being $0.65 < \lambda < 0.75$, the specific strain energy achieves its peak value owing to which chocks experience their compaction. Rigidity value of such protective structures depends upon the number of components of the wood construction.

It has been identified that in terms of the experimental samples subjected to uniaxial compression, there is exponential dependence with 0.95 correlation coefficient in the potential energy of shape change U_f – potential energy of volume change U_v ratio $\sigma^2 / 2 E_d$. It is obvious that the ratio value depends upon a lateral strain coefficient, i.e. upon physicomechanical characteristics of the protective structure material. The deformed body energy is higher, the lesser the lateral strain coefficient is. If increase in a lateral strain coefficient is up to $v = 0.3$ value then the behaviour of experimental samples under static loading in the context of uniaxial compression is mainly defined through changes in their shape. Such samples experience destruction with minor deformations (i.e. $\Delta h = 0.005$ m) at the expense of the sample main part shear towards another one. Before destruction, no sample has significant strain; it does not demonstrate any notable plastic deformations (Fig. 5a, b, c).

As for pliable protective structures under the conditions of uniaxial compression and static loading, compaction was preceded by the significant strain followed by certain changes in shape and volume (Fig. 5 d, and e).

Under loading, longitudinal compression of the samples was maximal, i.e. Δh = (0.026-0.03) m with minimal shape change U_f energy change in volume U_v ratio being $U_f / U_v = 2.1$.

Relying upon the abovementioned, it is possible to conclude that assessment of protective structures, involving their stability, rigidity, and bearing capacity, should be take into consideration their geometry (depending upon loading nature and type) as well as material characteristics.

Hence, pliable protective structures are more applicable to ensure both wall rock stability in the rock mass and operating conditions of mine workings. After compaction, such structures (for instance, in the form of wood chocks or sleeper chocks) are constructions with increasing resistance helping restrict displacement of wall rocks within the mined-out area of an extraction site.

To assess the efficiency of protective structures in the development mine workings, underground full-scale study is required. It will help analyze deformation processes, taking place in the coal-rock formation and influencing mine working stability along the extraction site length.

4. Conclusions

Resulting from the findings, comparative assessment has been made concerning strain characteristics of experimental samples under the conditions of uniaxial compression. Rigid protective structures in the form of coal pillars, cast strip, cement blocks, and BZBT piers were considered. Pliable protective structures were in the form of wood chocks, and wood sleeper chocks. External loading to pliable structures was applied perpendicularly to grain of wood components.

Under the conditions of uniaxial compression of the protective structures, exponential dependence is available between the ratio of potential energy of their changes and changes in volume energy, and the specific potential strain energy. The dependence helps identify bearing capacity of the protective structures in the development mine workings through variation in their rigidity. Hence, trouble-free operation of protective structures, which depends on the increase in structural resistivity without any loss of stability, is the basic reliability indicator of a procedure to protect the development mine workings.

Based upon the comparative analysis of strain characteristics of protective structures and processes, taking place during compression and impacting changes in shape, volume, and rigidity, the expediency to apply pliable wood structure has been identified. It has been determined that $0.65 \leq \lambda \leq 0.75$ changes in relative deformation of such protective structures ensure their stable state; in turn, rigidity depends upon the number of compressive elements and their arrangement. As for pliable protective structures, potential energy of changes in shape is 2.1 times more than energy of volume changes; the abovementioned favours their compaction. If rigid protective structures are applied and their relative strain exceeds $\lambda > (0.12 \div 0.15)$, i.e. it is beyond safe deformation resource, then they lose their stability and their rigidity drops by 14-22% preventing from restriction of wall rock displacement as well as failure within the workings of coal mines.

The research results may be used while substantiating the parameters of pliable protective structures to assess their bearing capacity as well as efficiency of the technique. To specify the parameters of protective structures, it is expedient to carry out full-scale studies in future which will help assess conditions of the development mine workings along the extraction site under real conditions of coal seam mining.

Acknowledgements

The authors thank the stuff of rock pressure laboratory of Donetsk National technical University for their assistance in the testing of experimental samples.

References

[1] Nikolin, V.I., Podkopayev, S.V., & Agafonov, A.V. (2005). *Snizheniye travmatizma ot proyavleniya gornogo davleniya*. Donetsk, Ukraina: Nord-press, 332 s.

[2] Tereshchuk, R.N., & Lozovsky, S.P. (2014). *Ustoychivost' podgotovitel'nykh vyrabotok s neustoychivoy pochvoy v zone vliyaniya ochistnykh rabot*. Dnipro, Ukraina: NGU, 103 s.

[3] Karkashadze, G.G. (2004). *Mekhanicheskoe razrushenie gornykh porod*. Moskva, Rossiya: MGGU Publ, 112 s.

[4] Parton, V.Z., & Morozov, E.M. (1974). *Mekhanika uprugoplasticheskogo razrusheniya*. Moskva, Rossiya: Nauka, 416 s.

[5] Kurdyumov, S.P. (2006). *Rezhimy s obostreniem. Evolyutsiya idei*. Moskva, Rossiya: Fizmatlit, 308 s.

[6] Sakhno, I., Sakhno, S.V., & Kamenets, V.I. (2022). Stress environment around head entries with pillarless godside entry retaining through numerical simulation incorporating the two type of filling wall. *IOP Conference Series: Earth and Environmental Science*, *1049*(1), 012011. https://doi.org/10.1088/1755-1315/1049/1/012011

[7] Yalanskiy, A.O., Slashchov, I.M., Slashchova, O.A., Seleznov, A.M., & Arestov, V.V. (2018). Development of new auxiliary measures for protecting preparatory roadways by the cast strips. *Geotechnical Mechanics*, (141), 3-17. https://doi.org/10.15407/geotm2018.141.003

[8] Negrey, S.G., Mokrienko, V.N., & Kurdyumov, D.N. (2013). Izuchenie vliyaniya formy okhrannogo sooruzheniya, vozvodimogo vdol' podgotovitel'noy vyrabotki, provedennoy vsled za lavoy, na mekhanizm smeshcheniy podstilayushchikh ego porod. *Prospects for the Development of Building Technologies*, 65-68.

[9] Nehrii, S., Nehrii, T., Zolotarova, O., Aben, K., & Yussupov, K. (2021). Determination of the parameters of local reinforced zones under the protection means. *E3S Web of Conferences*, (280), 08018. https://doi.org/10.1051/e3sconf/202128008018

[10] Nehrii, S., Nehrii, T., & Yefremov, I. (2020). Determination of parameters of detached rock packs with compensation voids. *Journal of Donetsk Mining Institute*, (2), 58-71. https://doi.org/10.31474/1999-981x-2020-2-58-71

[11] Zaslavsky, I.Yu., Kompaniets, V.F., Faivishchenko, A.G., & Kleschenkov, V.M. (1991). *Povyshenie ustoychivosti podgotovitel'nykh vyrabotok ugol'nykh shakht*. Moskva, Rossiya: Nedra, 235 s.

[12] Kazanin, O.I., Dolotkin, Yu.N., & Skrylnikov, I.V. (2011). Ispol'zovanie okhrannykh sooruzheniy dlya podderzhaniya vyemochnykh vyrabotok na ugol'nykh shakhtakh. *Mining Information and Analytical Bulletin*, (1), 34-39.

[13] Chen, H.P., & Doong, J.L. (1983). Postbuckling behavior of a thick plate. *AIA Journal*, *21*(8), 1157-1161. https://doi.org/10.2514/3.8220

[14] Hahn, H.T., & Williams, J.F. (1986). Compression failure mechanisms in unidirectional composites. *Composite Materials*, 115-139.

[15] Vildeman, V.E., & Tretyakov, V.P. (2013). Ispytaniya materialov s postroeniem polnykh diagramm deformirovaniya. *Problems of Mechanical Engineering and Reliability of Machines*, (5), 93-98.

[16] Cai, L., Wu, K., Qisheng, Y., & Jinpeng, F. (2011). A new method of equivalent material model deformation observation. *International Journal of Modern Education and Computer Science*, *3*(5), 40-46. https://doi.org/10.5815/ijmecs.2011.05.06

[17] Xie, G., Wang, L., & Luo, Y. (2010). Analysis on characteristics of damaged field of surrounding rock and face of FMTC. *Journal of Coal Science & Engineering (China)*, (16), 120-124. https://doi.org/10.1007/s12404-010-0202-x

[18] Cui, F., Jia, C., & Lai, X. (2019). Study on deformation and energy release characteristics of overlying strata under different mining sequence in close coal seam group based on similar material simulation. *Energies*, *12*(23), 4485. https://doi.org/10.3390/en12234485

[19] Taskinen, P., He, W., & Xu, Z. (2020). Study on law of overlying strata breakage and migration in downward mining of extremely close coal seams by physical similarity simulation. *Advances in Civil Engineering*, 2898971. https://doi.org/10.1155/2020/2898971

[20] Yang, H., Zhongping, G., Chen, D., Wang, C., Zhang, F., & Du, Z. (2020). Study on reasonable roadway position of working face under strip coal pillar in rock burst mine. *Rock Burst in Underground Engineering: Experiments and Analysis*, 8832791. https://doi.org/10.1155/2020/8832791

[21] Zhang, G., Guo, G., Lv, Y., & Gong, Y. (2020). Study on the strata movement rule of the ultrathick and weak cementation overburden in deep mining by similar material simulation: a case study in China. *Mathematical Problems in Engineering*, 7356740. https://doi.org/10.1155/2020/7356740

[22] Shashenko, A.N., Pustovoi, V.P., & Sdvizhnikova, E.A. (2015). *Geomekhanika*. Dnipro, Ukraina: 560 s.

[23] Inshibashi, I., & Hazarika, H. (2015). *Soil mechanics fundamentals and applications*. London, United Kingdom: CRC Press, 432 p. https://doi.org/10.1201/b18236

[24] Robitaille, V., & Tremblay, D. (2001). *Mecanique des sols: Theorie et pratique*. Paris, France: Modulo, 680 p.

[25] Tkachuk, O., Chepiga, D., Pakhomov, S., Volkov, S., Liashok, Y., Bachurina, Y., & Podkopaiev, S. (2023). Evaluation of the effectiveness of secondary support of haulage drifts based on a comparative analysis of the deformation characteristics of protective structures. *Eastern-European Journal of Enterprise Technologies*, *2*(1(122)), 73-81. https://doi.org/10.15587/1729-4061.2023.272454

[26] Stupishin, L.Yu. (2011). Variacionnyy kriteriy kriticheskikh urovney vnutrenney ehnergii deformacionnogo tela. *Industrial and Civil Construction*, (8), 21-23.

[27] Nasonov, I.D. (1978). *Modeling of mining processes*. Moscow, Russian Federation: Nedra, 204 p.

[28] Meshkov, Yu.Ya. (2001). *The concept of a critical density of energy in modern introduction to probability and statistics*. *Progress in Physics of Metals*, *2*(1), 7-50. https://doi.org/10.15407/ufm.02.01.007

[29] Barkovsky, V.V., Barkovsky, N.V., & Lopatin, O.K. (2002). *Teoriia ymovirnostei ta matematychna statystyka*. Kyiv, Ukraina: Tsentr uchbovoi literatury, 424 s.

[30] Cramer, H. (2016). Mathematical method of statistics. *Journal of Modern Physics*, *7*(9).

Деформація як процес трансформації форми та об'єму охоронних споруд підготовчих виробок при розвантаженні вуглепородного масиву

Д. Чепіга, І. Бессараб, В. Гнатюк, О. Ткачук, О. Кіпко, С. Подкопаєв

Мета. Оцінити деформаційні властивості охоронних споруд при розвантаженні вуглепородного масиву для забезпечення стійкості бічних порід та експлуатаційного стану підготовчих виробок у вугільних шахтах.

Методика. В умовах одновісного стиснення охоронних споруд на моделях в лабораторних умовах встановлено вплив деформаційних процесів на зміну їх жорсткості через трансформацію форми та об'єму.

Результати. В процесі деформування жорстких споруд у межах безпечного деформаційного ресурсу, потенціальна енергія їх формозміни значно (у 4.1-6.5 рази) перевищує потенціальну енергію зміни об'єму. За межами безпечного деформаційного ресурсу, коли перевищено критичний рівень питомої потенціальної енергії деформації, міцності охоронних споруд недостатньо для обмеження переміщень бічних порід, що обмежує їх застосування. При відносній зміні об'єму $\delta V > 0.06$-0.082 жорстких охоронних споруд, настає втрата їх стійкості. В таких умовах жорсткість конструкцій знижується на 14-22%. Для піддатливих охоронних споруд із дерева при відносній зміні об'єму $0.62 \leq \delta V \leq 0.72$ забезпечується зростання у 2 рази їх жорсткості. В таких умовах потенціальна енергія формозміни у 2.1 рази перевищує енергію зміни об'єму, що сприяє у часі ущільненню складових дерев'яних елементів стискаючої конструкції та підвищенню її опірності.

Наукова новизна. Встановлені закономірності зміни питомої потенціальної енергії деформації охоронних споруд від їх формозміни та зміни об'єму в умовах одновісного стиснення.

Практична значимість. Для забезпечення стійкості бічних порід та збереження експлуатаційного стану підготовчих виробок доцільно застосування охоронних піддатливих споруд з дерева, що дозволить після їх ущільнення обмежити переміщення покрівлі та підошви. Недостатня залишкова міцність жорстких охоронних споруд, яка настає після втрати їх стійкості, провокує обвалення порід на виїмкових дільницях вугільних шахт.

Ключові слова: *деформація, жорсткість, охоронні споруди, підготовчі виробки, одновісне стиснення, несуча здатність, потенціальна енергія*